CHIN. PHYS. LETT. Vol. 37, No. 8 (2020) 087103

Type-Ⅱ Dirac Semimetal State in a Superconductor Tantalum Carbide

Zhihai Cui(崔志海)[1,2], Yuting Qian(钱玉婷)[1,2], Wei Zhang(张薇)[3*],
Hongming Weng(翁红明)[1,2,4*], and Zhong Fang(方忠)[1,2]

[1]*Beijing National Research Center for Condensed Matter Physics, and Institute of Physics, Chinese Academy of Sciences, Beijing 100190, China*
[2]*School of Physical Sciences, University of Chinese Academy of Sciences, Beijing 100049, China*
[3]*Fujian Provincial Key Laboratory of Quantum Manipulation and New Energy Materials, College of Physics and Energy, Fujian Normal University, Fuzhou 350117, China*
[4]*Songshan Lake Materials Laboratory, Dongguan 523808, China*

(Received 12 June 2020; accepted 29 June 2020; published online 28 July 2020)

The exploration of topological Dirac semimetals with intrinsic superconductivity can be a most plausible way to discover topological superconductors. We propose that type-Ⅱ Dirac semimetal states exist in the band structure of TaC, a well-known s-wave superconductor, by using the first-principles calculations and the $\boldsymbol{k}\cdot\boldsymbol{p}$ effective model. The tilted gapless Dirac cones, which are composed of Ta d and C p orbitals and are protected by C_{4v} symmetry, are found to be below the Fermi level. The bands from Ta d orbitals are greatly coupled with the acoustic modes around the zone boundary, indicating their significant contribution to the superconductivity. The relatively high transition temperature ∼10.5 K is estimated to be consistent with the experimental data. To bring the type-Ⅱ Dirac points close to chemical potential, hole doping is needed. This seems to decrease the transition temperature a lot, making the realization of topological superconductivity impossible.

PACS: 71.20.−b, 74.25.−q, 73.20.At DOI: 10.1088/0256-307X/37/8/087103

Topological superconductors have emerged as one of the frontier topics of condensed matter physics, because they possess the long-sought-for Majorana fermions with zero-energy excitation, and can be potentially utilized for fault-tolerant topological quantum computation.[1−8] One of the possible candidates to realize the exotic topological superconductivity is Dirac semimetal (DSM), owing to its intrinsic nontrivial topology.[9−16] DSM, which is viewed as the three-dimensional version of graphene, has four-fold degenerate gapless nodal points with linear energy dispersion around them in momentum space. For the DSM system with both time-reversal symmetry (TRS) and inversion symmetry (P), single or double Dirac points can be obtained, protected by discrete rotation (C_n) symmetry.[6] Until now, superconductivity has been successfully revealed in several DSMs by theoretical prediction and experimental observation. For example, in Cd_3As_2,[17] Au_2Pb,[18] Fe(Se,Te),[4,19,20] Li(Fe,Co)As,[4,21] the Dirac points are protected by C_4 symmetry. Meanwhile, those of TMX_2 (TM = Ni, Pd, Pt; X = Se, Te) are protected by C_3 symmetry.[22] Therefore, DSM is a promising platform for exploring topological superconductivity, which is immune to nonmagnetic impurities.

TaC is a superconductor with a comparable high transition temperature $T_c \sim 10.6$ K.[23] Unfortunately, the physical mechanism of its superconductivity is still not very clear. In addition, TaC has notable properties, including a high melting point of 3983 ℃, high hardness of 15–19 GPa, high modulus of 537 GPa, and chemical resistance.[24] Furthermore, it is worth noting that TaC is in a rock salt structure and has C_4 symmetry. Thus, TaC may be one of the candidate materials for exploring topological superconductors.

In this letter, using first-principles calculations, symmetry analysis and the $\boldsymbol{k}\cdot\boldsymbol{p}$ effective model, we investigate the electronic properties, phonon properties and electron–phonon coupling (EPC), and report that type-Ⅱ DSM states exist in the superconducting TaC. In TaC, Ta d and C p orbitals consist of the gapless Dirac points with nontrivial topology. In addition, the Fermi surface nesting suggests that strong electron–phonon interaction leads to a possible Kohn anomaly, resulting in comparably high superconducting critical temperature ∼10.5 K. Therefore, TaC is a prominent candidate to explore intrinsic topological superconductivity and the related intriguing quantum

Supported by the National Natural Science Foundation of China (Grant Nos. 11974076, 11674369 and 11925408), and the Natural Science Foundation of Fujian Province of China (Grant No. 2018J06001), the Beijing Natural Science Foundation (Grant No. Z180008), Beijing Municipal Science and Technology Commission (Grant No. Z191100007219013), the National Key Research and Development Program of China (Grant Nos. 2016YFA0300600 and 2018YFA0305700), the K. C. Wong Education Foundation (Grant No. GJTD-2018-01), and the Strategic Priority Research Program of Chinese Academy of Sciences (Grant No. XDB33000000).
*Corresponding author. Email: zhangw721@163.com; hmweng@iphy.ac.cn
© 2020 Chinese Physical Society and IOP Publishing Ltd

properties.

Computation Method. In band structure calculations of TaC, we performed first-principles calculations using the VASP package[25,26] based on the density functional theory (DFT) with the projector augmented plane-wave (PAW) method.[27,28] The Perdew–Burke–Ernzerhof (PBE) exchange-correlation functional was used under generalized gradient approximation (GGA).[29] Spin–orbit coupling (SOC) was taken into account self-consistently. The cutoff energy for the plane-wave basis set was taken as 520 eV, and the Brillouin zone (BZ) sampling grid was a $20 \times 20 \times 20$ Monkhorst–Pack meshes in the self-consistent process for the ground state charge density.

Phonon dispersion was calculated by Quantum ESPRESSO[30] with the norm-conserving pseudopotentials.[31] The fully relaxed lattice parameters $a = b = c = 4.475$ Å were used. The self-consistent electron densities were evaluated on $10 \times 10 \times 10$ $\boldsymbol{k}$-point grids. The dynamical matrices as well as phonon perturbation potentials were calculated on an $8 \times 8 \times 8$ $\boldsymbol{q}$-mesh. The Wannier90[32] and EPW[33,34] codes were adopted to plot Fermi surface (FS) and interpolate an EPC constant. After the convergence test, finer electron (phonon) grids of $32 \times 32 \times 32$ ($16 \times 16 \times 16$) were used to interpolate the EPC. The maximally localized Wannier functions (MLWFs) were constructed for Ta d and C p orbitals.

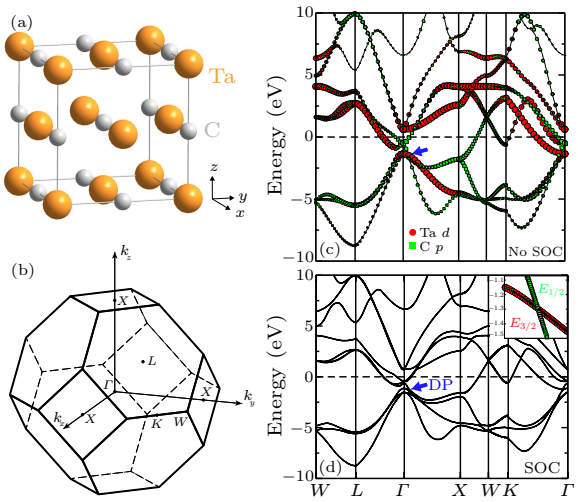

Fig. 1. Electronic structure of TaC from first-principles calculation and symmetry analysis. (a) Crystal structure. (b) Brillouin zone. (c) Orbital-resolved band structure calculated without SOC. A blue arrow represents an intersection along Γ–X direction. (d) Band structure with SOC. DP represents the tilted Dirac point along Γ–X direction. Orbital-resolved bands around the Dirac point with different irreducible representations are shown in the inset.

Results and Discussions. The transition metal carbide TaC is in rock salt structure, belonging to the space group O_h^5 ($Fm\bar{3}m$, No. 225). The crystal structure and BZ for TaC are shown in Figs. 1(a) and 1(b). Ta and C atoms are in position $4a(0,0,0)$ and $4b(1/2,1/2,1/2)$, respectively. The relaxed lattice constant 4.475 Å is used in the electronic structure calculation and the band structure is nearly similar to that with experimental lattice constant of 4.453 Å.[35]

We first study the band structure of TaC without SOC. Figure 1(c) shows that it is a typical metal with several bands crossing the Fermi level, leading to complex Fermi surfaces which will be discussed later in detail. Moreover, there exists a linear band intersection along Γ–X direction at -1.45 eV denoted by a blue arrow. The orbital-resolved band structure reveals that the band intersection is primarily contributed from two nondegenerate bands. One is composed of Ta d orbitals, while the other comes from the C p orbitals. Considering TRS and cubic symmetry, there are totally six such band intersections along $-X$–Γ and Γ–X directions as protected by C_{4v} symmetry. These band crossings originate from the band inversion between d and p states at Γ point, where the t_{2g} manifold of $5d$ orbitals (red dotted ones) are lower than the $2p$ orbitals (green squared ones) of C. In fact, these band crossings form three small entangled nodal rings around the Γ point without SOC. Further, the band structure with SOC considered is calculated as shown in Fig. 1(d). Without counting the spin degeneracy, at Γ both the triply degenerate t_{2g} orbitals and p orbitals have split into one double-degenerate and one single bands with effectively opposite SOC.[36] Though the hybridization of d–p orbitals is forbidden exactly at Γ, the effective SOC in $2p$ of C is enlarged much by Ta $5d$. The SOC splitting in $2p$ of C in TaC is about 0.231 eV, larger than that of 0.072 eV in NbC. SOC interaction also opens the band gap along the nodal rings and the other degenerate bands, but maintains six equivalent tilted Dirac points denoted by DP along Γ–X direction around -1.30 eV. Wave-function analysis illustrates that the crossing bands are described by different irreducible representations of C_{4v} point group:[37] the green fatted band is $E_{1/2}$, while that of the red fatted band is $E_{3/2}$, as shown in the inset of Fig. 1(d). The two branches of the Dirac point tilt so much that they have the same sign of velocities along Γ–X, forming a type-Ⅱ Dirac point.

To understand the fundamental properties of type-Ⅱ Dirac semimetal, the $\boldsymbol{k} \cdot \boldsymbol{p}$ Hamiltonian can be derived. Around the type-Ⅱ Dirac cone on the Γ–X line, the irreducible representations are $E_{1/2}$ and $E_{3/2}$ under the double group of C_{4v} symmetry. Therefore, the minimal Hamiltonian can be written as follows:[38]

$$H(\boldsymbol{k}) = \sum_{i,j=0}^{3} a_{ij}(\boldsymbol{k})\sigma_i\tau_j = \begin{pmatrix} h_{\uparrow\uparrow}(\boldsymbol{k}) & h_{\uparrow\downarrow}(\boldsymbol{k}) \\ h_{\downarrow\uparrow}(\boldsymbol{k}) & h_{\downarrow\downarrow}(\boldsymbol{k}) \end{pmatrix}, \quad (1)$$

where the σ_0 and τ_0 are identity matrices, $\sigma_{1,2,3}$ and $\tau_{1,2,3}$ are Pauli matrices for spin and orbital degree of freedom, respectively.

Based on the invariant theory, TRS, P and C_4 rotational symmetry require

$$\begin{aligned}
&\Theta H(\boldsymbol{k})\Theta^{-1} = H(-\boldsymbol{k}),\\
&PH(\boldsymbol{k})P^{-1} = H(-\boldsymbol{k}),\\
&C_4 H\left(k_+, k_-, k_z\right) C_4^{-1} = H\left(k_+ e^{i\frac{\pi}{2}}, k_- e^{-i\frac{\pi}{2}}, k_z\right),
\end{aligned} \tag{2}$$

where $k_\pm = k_x \pm i k_y$. TRS is represented by the operator $\Theta = i\sigma_2 K$, where K denotes complex conjugation. $P = \tau_z$ can be picked up as an inversion symmetry operator since the two crossing bands have even and odd parities at Γ, respectively. Choose Γ–X line as the rotation axis and C_4 can be represented by a diagonal matrix $C_4 = \mathrm{diag}[e^{i\frac{3\pi}{4}}, e^{i\frac{\pi}{4}}, e^{i\frac{-3\pi}{4}}, e^{i\frac{-\pi}{4}}]$ with the basis set in the order of J_z: $\frac{3}{2}$, $\frac{1}{2}$, $-\frac{3}{2}$, and $-\frac{1}{2}$.

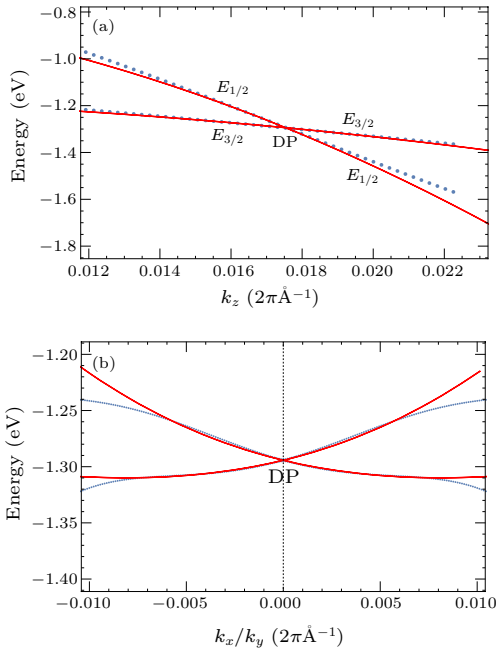

Fig. 2. The fitted band structure around the Dirac point (DP) of TaC along the k_z direction (a) and k_x (k_y) direction (b). The blue dotted lines represent the band structure obtained from first-principles calculations and the red lines are from the $\boldsymbol{k}\cdot\boldsymbol{p}$ model. The irreducible representations of $E_{1/2}$ and $E_{3/2}$ under the double group of C_{4v} symmetry on the Γ–X line form the type-Ⅱ Dirac cone.

Therefore, the low-energy effective Hamiltonian respecting these symmetries can be expressed as

$$H(\boldsymbol{k}) = \begin{pmatrix} D_1 & A & 0 & B \\ & D_2 & B & 0 \\ & & D_1 & -A^* \\ \dagger & & & D_2 \end{pmatrix}, \tag{3}$$

where

$$\begin{aligned}
&A = 2\eta k_+,\\
&B = 2\left(\delta k_+^2 + \xi k_-^2\right) k_z,\\
&D_1 = (\alpha_0 + \alpha_5) + (\beta_0 + \beta_5)\, k_+ k_- + (\gamma_0 + \gamma_5)\, k_z^2,\\
&D_2 = (\alpha_0 - \alpha_5) + (\beta_0 - \beta_5)\, k_+ k_- + (\gamma_0 - \gamma_5)\, k_z^2,
\end{aligned} \tag{4}$$

and α_n, β_n, γ_n and η, δ, ξ are real numbers and complex numbers, respectively.

Figure 2 shows the fitted band structure of the $\boldsymbol{k}\cdot\boldsymbol{p}$ model. The fitting parameters $\alpha_0 = -0.960$, $\alpha_5 = 0.207$, $\beta_0 = 7.929$, $\beta_5 = -0.378$, $\gamma_0 = -27.544$, $\gamma_5 = -17.052$, $\eta = 0.330 + 0.002i$, $\delta = 23.294 + 1.971i$, and $\xi = 0.003 - 0.383i$ were used to diagonalize $H(\boldsymbol{k})$. The calculation shows a clear type-Ⅱ Dirac band dispersion with a four-fold degenerate Dirac point [Fig. 2(a)]. We also check the band structures along k_x and k_y directions in the vicinity of Dirac point [Fig. 2(b)], which are very consistent with our DFT results.

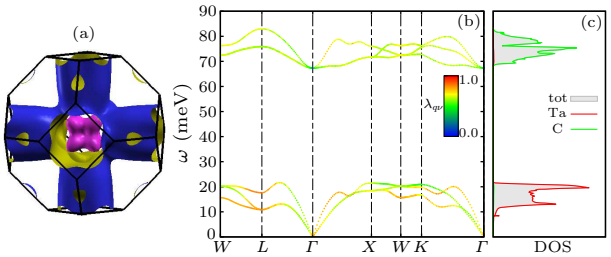

Fig. 3. (a) Fermi surface for TaC without SOC. (b) Phonon dispersion along high-symmetry line with colors representing $\lambda_{\boldsymbol{q}\nu}$ at a specific wave vector and mode. (c) Projected phonon density of states.

Next, we concentrate on the phonon structure and superconductivity. TaC has been reported to be a superconductor with transition temperature T_c of 10.6 K.[23] To further investigate the superconductivity of TaC, we calculate the FS and EPC strength using the DFT and the Wannier interpolation technique. As shown in Fig. 3(a), there are six arms lying along the Γ–X direction which contribute to possible Fermi nesting vectors, resulting in Kohn anomalies in acoustic modes.[39,40] This has been studied to be related to the superconductivity of transition metal carbides. The calculated phonon dispersion is shown in Fig. 3(b). No observed imaginary phonon frequency suggests that it is a dynamically stable phase. The calculated projected phonon density of states shown in Fig. 3(c) suggests that the acoustic modes are mainly from the contribution of Ta atoms, and the optical modes from C atoms. This may result from the mass ratio of $m_{\mathrm{Ta}}/m_{\mathrm{C}} \sim 15$. We calculate the EPC constant $\lambda_{\boldsymbol{q}\nu}$ by

$$\lambda_{\boldsymbol{q}\nu} = \frac{2}{\hbar N_{\mathrm{F}} N_{\boldsymbol{k}}} \sum_{nm\boldsymbol{k}} \frac{1}{\omega_{\boldsymbol{q}\nu}} |g^{nm}_{\boldsymbol{k},\boldsymbol{q}\nu}|^2 \delta(\epsilon^n_{\boldsymbol{k}}) \delta(\epsilon^m_{\boldsymbol{k}+\boldsymbol{q}}), \tag{5}$$

and EPC constant λ by summing over momentum $\boldsymbol{q}$ and mode ν in the first BZ:

$$\lambda = \frac{1}{N_{\boldsymbol{q}}} \sum_{\boldsymbol{q}\nu} \lambda_{\boldsymbol{q}\nu}, \tag{6}$$

where $N_{\boldsymbol{k}}$ and $N_{\boldsymbol{q}}$ are total number of $\boldsymbol{k}$ and $\boldsymbol{q}$ points in finely sampled grids, respectively. N_{F} is the density of states of electrons at Fermi level. Here $\omega_{\boldsymbol{q}\nu}$ is the

phonon frequency, $g^{nm}_{\boldsymbol{k},\boldsymbol{q}\nu}$ is the electron–phonon vertex, and δ is the Dirac delta function; $\epsilon^{n}_{\boldsymbol{k}}$ ($\epsilon^{m}_{\boldsymbol{k}+\boldsymbol{q}}$) is the eigenvalue of Kohn–Sham wavefunction with crystal momentum $\boldsymbol{k}$ ($\boldsymbol{k}+\boldsymbol{q}$) and band index $n(m)$.

The superconducting transition temperature $T_{\rm c}$ can be estimated by the McMillan–Allen–Dynes formula[41]

$$T_{\rm c} = \frac{\omega_{\log}}{1.2}\exp\left[\frac{-1.04(1+\lambda)}{\lambda(1-0.62\mu^*)-\mu^*}\right], \tag{7}$$

with $\omega_{\log} = \exp\langle\ln\omega\rangle$, and μ^* is the Coulomb pseudopotential. The colored phonon dispersion weighted with different EPC strength $\lambda_{\boldsymbol{q}\nu}$ is shown in Fig. 3(b). It can be seen that the acoustic modes from Ta atoms vibration around zone boundary L, along Γ–X and Γ–K have stronger EPC than the optical modes from C atoms. This is consistent with the fact that the Fermi surfaces having these nesting vectors corresponding to these phonon vectors are mostly composed of 5d orbits of Ta atoms, as shown in Fig. 1(c). Summing $\lambda_{\boldsymbol{q}\nu}$ over the first BZ on a fine $\boldsymbol{q}$-mesh, we can obtain EPC constant $\lambda = 0.92$. $T_{\rm c}$ of TaC can be obtained to be about 10.5 K with $\mu^* = 0.18$ in order to agree with the available experimental temperature value 10.6 K. Since the type-Ⅱ Dirac points are at -1.30 eV below the Fermi level, it is better to dope TaC with holes so that the chemical potential closes to Dirac points. It has been found that if hole doping is introduced into TaC, the EPC will decrease to the value close to that of HfC[39] and HfC has superconducting transition temperature less than 0.1 K. This makes the topological superconductivity in TaC quite unplausible.

In summary, our first-principles calculations and symmetry analysis reveal that the TaC in rock salt structure has six type-Ⅱ tilted Dirac cones, protected by C_{4v} symmetry, along the Γ–X paths below the Fermi level. A $\boldsymbol{k}\cdot\boldsymbol{p}$ effective model further reproduces the Dirac points with Ta d orbitals and C p orbitals as basis set. Moreover, phonon calculations confirm that the structure is dynamically stable. The electron–phonon coupling is mainly contributed by the Fermi surfaces, which are composed of Ta 5d bands hosting acoustic phonons with vectors around the zone boundary. The Fermi surfaces from C 2p bands and the optical modes from C atoms have quite a small contribution to electron–phonon coupling. The estimated superconducting transition temperature for TaC ∼10.5 K is very consistent with the experimental result ∼10.6 K. Hole doping can bring the type-Ⅱ Dirac points close to Fermi level, while the electron–phonon coupling decreases. The decreased electron–phonon coupling may lead to quite low superconducting transition temperature. Thus, the topological superconductivity is unlikely to be realized.

Note added. After the submission of this manuscript, we became aware of the related work by Shang *et al.*,[42] in which TaC is proposed to host nontrivial topological band structure coexisting with superconductivity.

References

[1] Qi X L and Zhang S C 2011 *Rev. Mod. Phys.* **83** 1057
[2] Nayak C, Simon S H, Stern A, Freedman M and Das Sarma S 2008 *Rev. Mod. Phys.* **80** 1083
[3] Fu L and Kane C L 2008 *Phys. Rev. Lett.* **100** 096407
[4] Kawakami T and Sato M 2019 *Phys. Rev. B* **100** 094520
[5] Zhang J L, Zhang S J, Weng H M, Zhang W, Yang L X, Liu Q Q, Feng S M, Wang X C, Yu R C, Cao L Z, Wang L, Yang W G, Liu H Z, Zhao W Y, Zhang S C, Dai X, Fang Z and Jin C Q 2011 *Proc. Natl. Acad. Sci. USA* **108** 24
[6] Kobayashi S and Sato M 2015 *Phys. Rev. Lett.* **115** 187001
[7] Qian Y, Nie S, Yi C, Kong L, Fang C, Qian T, Ding H, Shi Y, Wang Z, Weng H and Fang Z 2019 *npj Comput. Mater.* **5** 121
[8] Jia Y T, Zhao J F, Zhang S J, Yu S, Dai G Y, Li W M, Duan L, Zhao G Q, Wang X C, Zheng X, Liu Q Q, Long Y W, Li Z, Li X D, Weng H M, Yu R Z, Yu R C and Jin C Q 2019 *Chin. Phys. Lett.* **36** 087401
[9] Wang Z, Sun Y, Chen X Q, Franchini C, Xu G, Weng H, Dai X and Fang Z 2012 *Phys. Rev. B* **85** 195320
[10] Wang Z, Weng H, Wu Q, Dai X and Fang Z 2013 *Phys. Rev. B* **88** 125427
[11] Young S M, Zaheer S, Teo J C Y, Kane C L, Mele E J and Rappe A M 2012 *Phys. Rev. Lett.* **108** 140405
[12] Wan X, Turner A M, Vishwanath A and Savrasov S Y 2011 *Phys. Rev. B* **83** 205101
[13] Xu G, Weng H, Wang Z, Dai X and Fang Z 2011 *Phys. Rev. Lett.* **107** 186806
[14] Zhang W, Luo K, Chen Z, Zhu Z, Yu R, Fang C and Weng H 2019 *npj Comput. Mater.* **5** 105
[15] Zhang W, Wu Q, Yazyev O V, Weng H, Guo Z, Cheng W D and Chai G L 2018 *Phys. Rev. B* **98** 115411
[16] Wu M, Zhang H, Zhu X, Lu J, Zheng G, Gao W, Han Y, Zhou J, Ning W and Tian M 2019 *Chin. Phys. Lett.* **36** 067201
[17] Wang H, Wang H, Liu H, Lu H, Yang W, Jia S, Liu X J, Xie X C, Wei J and Wang J 2016 *Nat. Mater.* **15** 38
[18] Schoop L M, Xie L S, Chen R, Gibson Q D, Lapidus S H, Kimchi I, Hirschberger M, Haldolaarachchige N, Ali M N, Belvin C A, Liang T, Neaton J B, Ong N P, Vishwanath A and Cava R J 2015 *Phys. Rev. B* **91** 214517
[19] Wang D, Kong L, Fan P, Chen H, Zhu S, Liu W, Cao L, Sun Y, Du S, Schneeloch J, Zhong R, Gu G, Fu L, Ding H and Gao H J 2018 *Science* **362** 333
[20] Machida T, Sun Y, Pyon S, Takeda S, Kohsaka Y, Hanaguri T, Sasagawa T and Tamegai T 2019 *Nat. Mater.* **18** 811
[21] Liu Q, Chen C, Zhang T, Peng R, Yan Y J, Wen C H P, Lou X, Huang Y L, Tian J P, Dong X L, Wang G W, Bao W C, Wang Q H, Yin Z P, Zhao Z X and Feng D L 2018 *Phys. Rev. X* **8** 041056
[22] Zhang J and Huang G Q 2020 *J. Phys.: Condens. Matter* **32** 205702
[23] Zeller H R 1972 *Phys. Rev. B* **5** 1813
[24] Zhang X, Hilmas G E, Fahrenholtz W G and Deason D M 2007 *J. Am. Ceram. Soc.* **90** 393
[25] Kresse G and Hafner J 1993 *Phys. Rev. B* **48** 13115
[26] Kresse G and Furthmüller J 1996 *Comput. Mater. Sci.* **6** 15
[27] Blöchl P E 1994 *Phys. Rev. B* **50** 17953
[28] Kresse G and Joubert D 1999 *Phys. Rev. B* **59** 1758
[29] Perdew J P, Burke K and Ernzerhof M 1996 *Phys. Rev. Lett.* **77** 3865
[30] Giannozzi P, Baroni S, Bonini N, Calandra M, Car R, Cavazzoni C, Ceresoli D, Chiarotti G L, Cococcioni M, Dabo I, Dal Corso A, de Gironcoli S, Fabris S, Fratesi G,

Gebauer R, Gerstmann U, Gougoussis C, Kokalj A, Lazzeri M, Martin-Samos L, Marzari N, Mauri F, Mazzarello R, Paolini S, Pasquarello A, Paulatto L, Sbraccia C, Scandolo S, Sclauzero G, Seitsonen A P, Smogunov A, Umari P and Wentzcovitch R M 2009 *J. Phys.: Condens. Matter* **21** 395502
[31] Troullier N and Martins J L 1991 *Phys. Rev. B* **43** 1993
[32] Mostofi A A, Yates J R, Lee Y S, Souza I, Vanderbilt D and Marzari N 2008 *Comput. Phys. Commun.* **178** 685
[33] Noffsinger J, Giustino F, Malone B D, Park C H, Louie S G and Cohen M L 2010 *Comput. Phys. Commun.* **181** 2140
[34] Poncé S, Margine E R, Verdi C and Giustino F 2016 *Comput. Phys. Commun.* **209** 116
[35] Nakamura K and Yashima M 2008 *Mater. Sci. & Eng. B* **148** 69
[36] Sheng X L, Wang Z, Yu R, Weng H, Fang Z and Dai X 2014 *Phys. Rev. B* **90** 245308
[37] Altmann S and Herzig P 1994 *Point-Group Theory Tables* (Oxford: Clarendon)
[38] Yang B J and Nagaosa N 2014 *Nat. Commun.* **5** 4898
[39] Noffsinger J, Giustino F, Louie S G and Cohen M L 2008 *Phys. Rev. B* **77** 180507
[40] Blackburn S, Côté M, Louie S G and Cohen M L 2011 *Phys. Rev. B* **84** 104506
[41] Allen P B and Dynes R C 1975 *Phys. Rev. B* **12** 905
[42] Shang T, Zhao J Z, Gawryluk D J, Shi M, Medarde M, Pomjakushina E and Shiroka T 2020 *Phys. Rev. B* **101** 214518